Rare Metal Materials and Engineering
Volume 49, Issue 10, October 2020
Available online at www.rmme.ac.cn

Science Press

Cite this article as: Rare Metal Materials and Engineering, 2020, 49(10): 3338-3346.

ARTICLE

Effect of Impurity Elements (C, Si) on Microstructure and Corrosion Resistance of Zircaloy-4 Sheet

Chu Linhua[1], Yuan Gaihuan[1], Yao Meiyi[2], Gao Bo[1], Xu Shitong[2], Zhou Bangxin[2]

[1] State Nuclear Bao Ti Zirconium Industry Company, National R&D Center of Nuclear Grade Zirconium Material, Shaanxi Key Laboratory of Nuclear Grade Zirconium Material, Baoji 721013, China; [2] Shanghai University, Shanghai 200072, China

Abstract: In the range of ASTM, the effect of impurity elements on microstructure and corrosion resistance of Zr-4 alloy was studied by using sheet samples. The results show that reducing carbon content and increasing silicon content are beneficial to improve uniform corrosion resistance of Zr-4 alloy at 400 °C steam. Microscopic analysis shows that carbon is easily enriched in the form of Zr-C on the matrix phase, and it mainly affects the corrosion resistance by influencing the precipitation of second phase particles. The lower its content is, the easier it is to form the parallel plate (PP) structure during quenching, and the higher its content is, the more likely it is to form basket weave (BW) structure, while the second phase particles are easier to precipitate along the grain boundary of PP structure. When quenching temperature is lower than 1200 °C, silicon content has no obvious effect on the formation of PP structure. Meanwhile, three-dimensional atom probe (3DAP) analysis shows that silicon tends to agglomerate in the form of SiO_2 around the second phase particles, and delays or weakens the oxidation of second phase particles, thus improving the corrosion resistance of Zr-4 alloy.

Key words: zircaloy; impurity; microstructure; uniform corrosion; β-solution treatment; second phase particles; agglomerate

Zircaloy-4 is widely used as pressurized water reactor structure materials because of its excellent corrosion resistance. Many works have been reported to investigate the relationship between the corrosion resistance and the composition[1-4], process parameters[5-8], and cumulative annealing parameter A value[9-12] of the Zr-4 alloy.

Thorvaldsson et al[13] introduced that the uniform general corrosion behavior of Zircaloy-4 has been determined in long-term autoclave tests at 400 °C and modeled using the annealing parameter A concept. The cumulative effect of subsequent heat treatments in the alpha phase field after beta quenching can be given by $A=\sum_i t_i \exp(Q/RT_i)$, where t_i is annealing time, T_i is the temperature, Q is the activation energy, and R is the gas constant. Charquet et al[14] pointed out that the nodular corrosion was easier to satisfy by increasing the cooling rate, while the better uniform performance must be combined with the appropriate A value. The A value mainly affects the corrosion resistance of Zr-4 alloy by restricting the size and quantity of the second phase particles. Different scholars have various results based on their own experiments. Maussner et al[15] introduced that the ideal nodular corrosion performance requires the second phase particles' diameter does not exceed 200 nm. Garazarolli et al[16] determined the optimal A value range of 2×10^{-18}~5×10^{-17} h. In addition, Foster[17], Sabol[18] and Cao[19] also obtained the best A value and the second phase particles' size range based on their separate experiments. These results are different, but all show that the appropriate process window is narrow without optimizing the composition.

Eucken et al[20] reported that increasing the content of tin and carbon increases corrosion, while increasing the content of iron, chromium, and silicon shows a beneficial effect on uniform corrosion. The effect of the chemical composition on nodular corrosion is qualitatively the same as the effect on uniform corrosion for tin, iron, chromium, and carbon, whereas silicon shows an opposite behavior. For oxygen and phosphorus, there is only an influence at high temperatures (500 °C). As for the influence of alloying elements on

Received date: October 18, 2019
Corresponding author: Chu Linhua, Ph. D., Senior Engineer, State Nuclear Bao Ti Zirconium Industry Company, Baoji 721013, P. R. China, Tel: 0086-917-8661613, E-mail: chulinhuascu@163.com

microstructure, Luan et al[21] found that it tended to form the basket weave (BW) structure when the content of C is high; on the contrary, it is easy to form the parallel plate (PP) structure. Charquet et al[14] pointed out that when the quenching temperature is lower than 1200 °C, Si content has no obvious effect on the formation of parallel plate (PP) structure. Although many works have clearly pointed out the relationship of C, Si, and P content on the quenching microstructures, there have been no reports that it is directly related to the corrosion performance.

In this paper, the effects of different proportions of Sn, Fe, Cr, C, Si elements on corrosion behavior were investigated by preparing sheet samples of Zr-4 alloy. In particular, the effects of C and Si content on the microstructures and distribution of second phase particles were mainly studied. The relationship between them and corrosion performance was further explained.

1 Experiment

The sheet samples used in this study were melted into about 25 kg button ingots with 160 mm in diameter. Three melting cycles were performed in order to ensure the chemical homogeneity. Table 1 summarizes the chemical composition of different alloying elements. Tin, iron, chromium and silicon were tested on the SPECTRO ARCOS inductively coupled plasma optical emission spectrometer (ICP-OES). A CS600 carbon and sulfur analyzer was used to analyze the carbon content of sheet samples. All of them were controlled in the ASTM range.

The button ingots were converted to about 1.0 mm thick sheets by standard zirconium-alloy processing sequence (as shown in Fig.1), consisting of β-forging at 1030 °C, β-quenching at 1030 °C, α-hot rolling at 640 °C, cold-rolling in several steps with intermediate α-annealing at 640 °C for 3~5 h. Sheet materials were finally annealed in fully recrystallized conditions.

In order to compare the effects of different composition design on the corrosion performance, long-term corrosion test was performed on the sheet samples in steam at 400 °C for 300 d at a pressure of 10.3 MPa using the static autoclaves. And the appearance and mass gain were observed. Meanwhile, the samples were accelerated testing for 150 d at 420 °C[22]. The quenching microstructures of sheet samples with different compositions were observed by Leica DM2500M metallographic microscope. The size, quantity and distribution of second phase particles in the sheet samples were analyzed by using a 200CX transmission electron microscope (TEM). With the help of LEAP3000HR three-dimensional atom probe (3DAP), the segregation of elements on the sample's surface was analyzed. The tip sample was prepared by 600I type double-beam focused ion beam system (FIB). ESCALAB250Xi multifunctional X-ray photoelectron spectrometer (XPS) was used to explore the segregation of elements on the matrix phase.

2 Results and Discussion

2.1 Effect of composition on the corrosion

Typical mass gain versus time curves for the sheet samples

Table 1 Chemical composition of 1#~9# sheet samples (wt%)

Sheet sample No.	Sn	Fe	Cr	Fe+Cr	C	Si
1#	1.30	0.20	0.10	0.30	0.0035	0.0015
2#	1.30	0.20	0.11	0.30	0.0035	0.0100
3#	1.30	0.20	0.10	0.30	0.0120	0.0101
4#	1.31	0.21	0.10	0.31	0.0125	0.0015
5#	1.31	0.20	0.10	0.30	0.0122	0.0065
6#	1.55	0.20	0.10	0.30	0.0123	0.0100
7#	1.30	0.23	0.12	0.35	0.0121	0.0102
8#	1.31	0.23	0.12	0.35	0.0034	0.0103
9#	1.31	0.20	0.11	0.31	0.0075	0.0098
ASTM	1.20~1.70	0.18~0.24	0.09~0.13	0.27~0.37	＜0.0200	＜0.0120

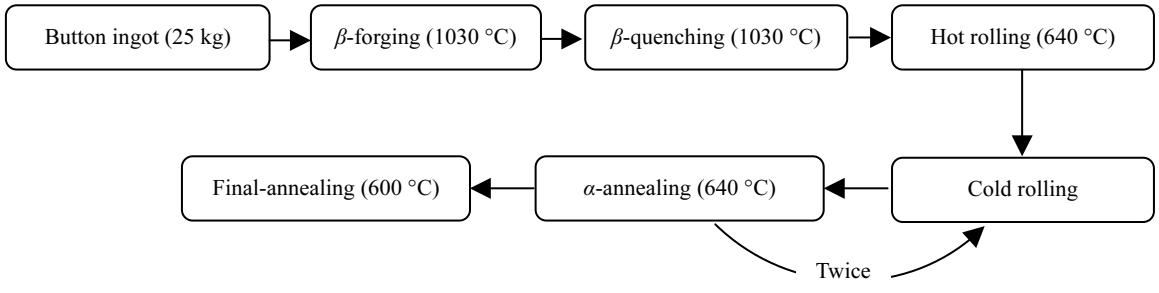

Fig.1 Processing sequence of investigated sheet materials

with different C contents tested in steam at 400 and 420 °C are given in Fig.2a. As shown in the figure, when the content of Sn (1.30 wt%), Si (0.01 wt%) and Fe+Cr (0.30 wt%) is fixed, with the increase of C content, the sheets' corrosion rate increases continuously under two corrosion conditions. It also can be concluded that the decreasing of C content is beneficial for improving the corrosion resistance of sheet samples.

Fig.3a~3c show the surface of sheet samples with different C contents which have been exposed in steam at 400 °C for 300 d. It can be seen that the samples' surface with a low C content is still dark and bright, while other samples with a higher C content exhibit a large amount of gray spots, which have been confirmed to be ZrO_2.

The effect of Si content on the corrosion rate of sheet samples tested in steam at 400 and 420 °C is shown in Fig.2b. Contrary to the influence of C content, the sheets' corrosion rate reduces continuously under two conditions with the increase of Si content. The appearance of three sheet samples exposed in steam at 400 °C for 300 d shown in Fig.3d~3f has further demonstrated the results. The samples' surface with a high Si content is still dark and bright, while other samples with a lower Si content exhibit a large amount of gray spots.

The mass gain versus time curves for the sheet samples with different Sn and Fe+Cr contents tested in steam at 400 °C are given in Fig.2c. When the content of C (0.012wt%) and Si (0.010wt%) is fixed, the sheets' mass gain rate increases with the increases of Sn, and decreases with the increases of Fe+Cr. However, since high C is used, the four samples have poor long-term uniform corrosion performance and little difference from each other, which further indicates that high C content is

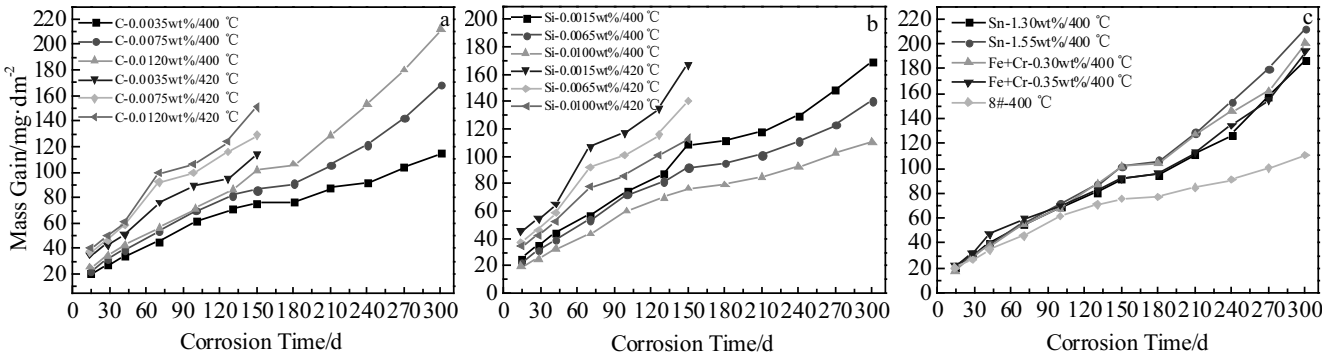

Fig.2 Mass gains as a function of C (a), Si (b) and Sn and Fe+Cr (c) contents tested in steam at 400 °C for 300 d and 420 °C for 150 d

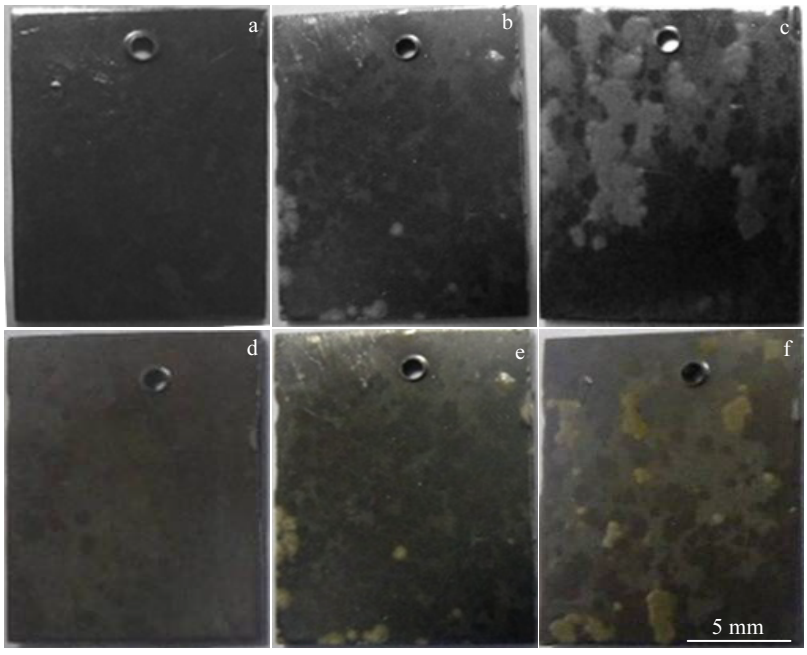

Fig.3 Surface morphologies of sheet samples with different C and Si contents tested in steam at 400 °C for 300 d: (a) 0.0035wt% C, (b) 0.0075wt% C, (c) 0.0120wt% C; (d) 0.0100wt% Si, (e) 0.0065wt% Si, and (f) 0.0015wt% Si

extremely unfavorable to uniform corrosion performance. The sample No.8 is designed with 'low C+ high Si' composition, which shows the best corrosion resistance. In the industrial production, it is difficult to stably control the contents of Sn, Fe and Cr in a certain range without exceeding ASTM standard. Therefore, the key to obtain Zr-4 alloy products with excellent corrosion resistance is to strictly control the contents of impurity elements, especially C and Si.

2.2 Microstructure analysis

Fig.4 shows the distribution and statistical results of second phase particles in the sheet samples with different C and Si contents analyzed by TEM. From the comparison between Fig.4a and 4b, it can be found that the area fraction of second phase particles increases from 0.82% to 1.61%, and the average diameter increases from 65 nm to 75 nm with the increase of Si content, which indicates that the increase of Si content obviously promotes the precipitation of second phase particles. Meanwhile, comparing Fig.4b with 4c, the area fraction decreases from 1.61% to 1.01%, and the average diameter decreases to 58 nm due to the increase of C content in the case of high Si content, indicating that the increase of C content significantly inhibits the precipitation of second phase particles.

In order to explain the effect mechanism of C and Si contents on the distribution of second phase particles in the sheet samples, the quenching process was retrospectively analyzed. Fig.5 shows the comparison of quenching microstructures and second phase particles of billets with different C and Si contents. As shown in Fig.5a, when the content of C is high, a large number of nucleation sites (Zr-C particles of fcc structure) are provided for the α phase inside the β grain. Due to the symmetry of the cubic β-Zr, the α lath can grow on a plurality of eutectoid surfaces, and is cut off by other α laths growing at the same time before being long, thus forming a parallel plate structure[23]. As shown in Fig.5b, when the content of C is low, these nucleation sites are rare or non-existent. The α lath starts to grow from the β-phase grain boundary. Because only one eutectoid surface is most favorable for growth, a group of such α laths grow together into the β grain, finally forming a crisscross basket weave structure. In addition, according to the report[14], when the solution temperature is lower than 1200 °C, the content of Si has no obvious influence on the type of quenching microstructures.

As shown in Fig.5c~5f, a large number of second phase particles ($Zr(FeCr)_2$) can precipitate freely along the grain boundaries of parallel plate structure. However, it seems difficult to precipitate in the basket weave structure. Although the billet still needs to undergo a series of heat treatment processes, these processes can only change the size of second phase particles to a certain extent, and it is difficult to affect the quantity. Meanwhile, according to the report[14], compared to the basket weave structure, the parallel plate structure seems to be more easily broken in the subsequent rolling process, thus facilitating the secondary precipitation of second phase particles. Therefore, it can be concluded that the C content affects the initial quenching microstructures and precipitation of second phase particles, and thus affects the

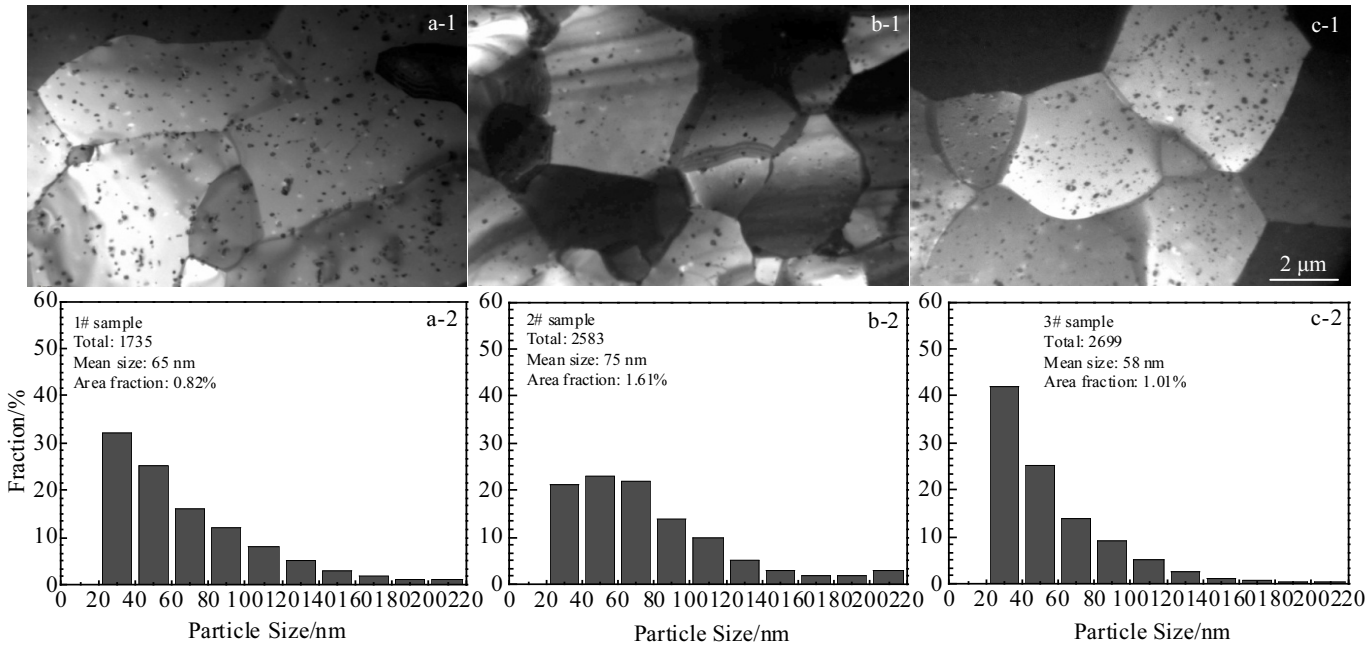

Fig.4 Distribution of second phase particles in the sheet samples with different C and Si contents: (a) C-0.0035 wt%, Si-0.0015 wt%; (b) C-0.0035 wt%, Si-0.010 wt%; (c) C-0.012 wt%, Si-0.010 wt%

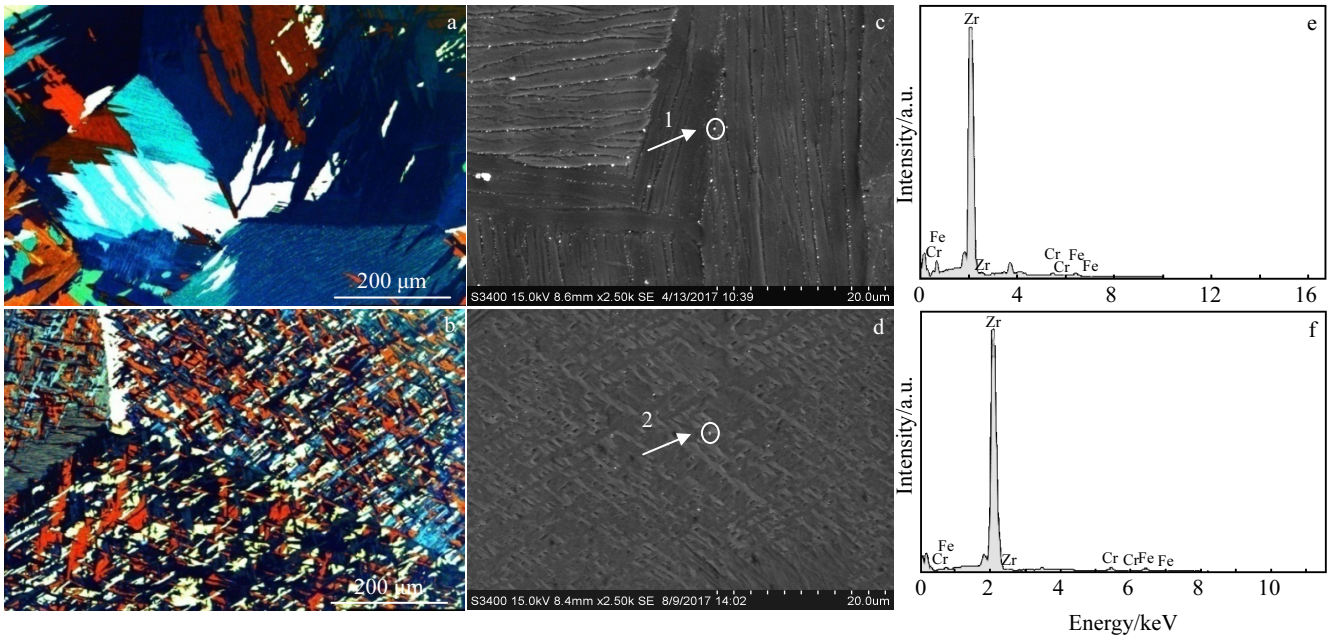

Fig.5 Quenching microstructures and second phase particles of billets with different C and Si contents: (a) PP structure; (b) BW structure; (c) SPP along PP structure boundary; (d) SPP in the BW structure; (e) EDS spectrum of point 1 in Fig5c; (f) EDS spectrum of point 2 in Fig.5d

corrosion resistance of Zr-4 alloy.

For the sheet samples with low C and high Si, the segregation of elements on the interface was analyzed by 3DAP. As can be seen from Fig.6, there are two areas with different Fe and Cr contents: enrichment area and barren area. In order to distinguish the two regions, one-dimensional concentration distribution map was made along the arrow direction in Fig.7, and the iso-concentration surface of Fe and Cr are obtained as shown in Fig.7b and 7c, respectively, with the Fe concentration 2at%, and the Cr concentration 2.5at%. In the one-dimensional concentration distribution diagram of C and Si (Fig.8), it is observed that Si has segregation on the interface of second phase and matrix phase.

In order to explore the segregation of C and Si elements in the sample, XPS was used to continue in-depth analysis of low C and high Si samples. Pickling treatment before the test can remove surface pollution, but also destroy the information of sample surface, so each sample was compared with two groups of data of pickling and non-pickling.

The Si fine spectra of pickled and un-pickled samples etched for different time are shown in Fig.9a and 9b. It can be seen that there is a characteristic peak with a binding energy of about 101 eV (as shown by arrow 1 in Fig.9a) when the pickled samples are etched for 0 s, when Si exists in the form of SiO_2. When samples are etched for 1150 s, there is a characteristic peak with a binding energy of about 97 eV (as shown by arrow 2 in Fig.9a), when Si exists in the form of monatomic silicon. No characteristic peak of Si is detected

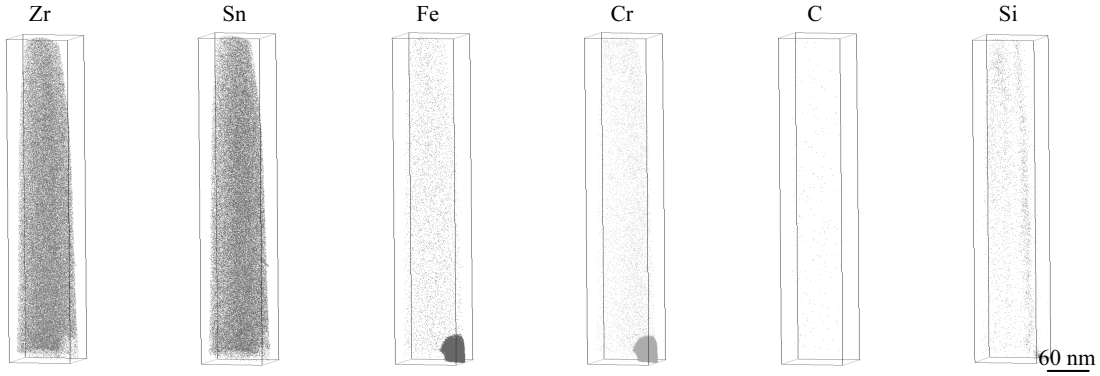

Fig.6 Different atomic three-dimensional space distribution maps

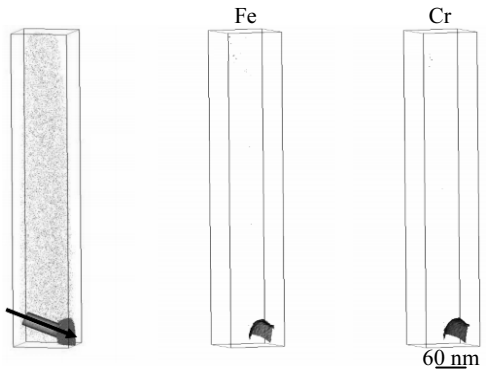

Fig.7 Atomic three-dimensional space distribution maps

after etching is continued. The characteristic peak with a binding energy of about 101 eV exists in the un-etched sample during etching for 0 s to 1150 s, and the intensity of characteristic peak gradually decreases with the increase of etching time (as shown by arrows 1~4 in Fig.9b), when Si exists in the form of SiO_2. When etching for 0~1150 s, there is a characteristic peak with a binding energy of about 98 eV (as shown by arrows 5~8 in Fig.9b), and Si exhibits the form of monatomic silicon. No characteristic peak of Si is detected after 1150 s etching. This further indicates that Si does indeed agglomerate on the matrix surface.

The C fine spectra of pickled and un-pickled samples etched for different time are shown in Fig.9c and 9d. It can be seen that there is a characteristic peak with a binding energy of 284.8 eV (as shown by arrow 1 in Fig.9c and 9d) on the surface of both samples etched for 0 s, when C exists in the form of C-C adsorption. A characteristic peak with a binding energy of about 282 eV exists in the un-etched sample after 60 s of etching. At this time, the adsorbed C on the surface has been removed, and C exists in the bound state (Zr-C, B.E.=282.1 eV). This further indicates that C does have surface segregation.

2.3 Relationship between microstructure and corrosion performance[24-26]

Regarding the mechanism of how the composition and *A*

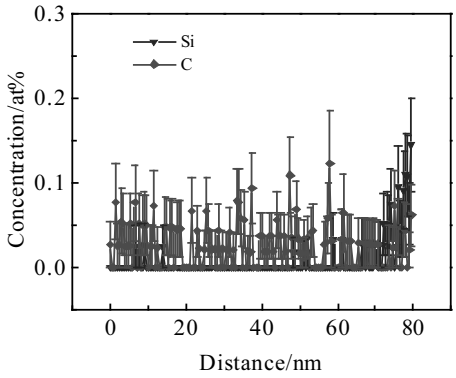

Fig.8 One dimensional concentration distribution of C and Si in the arrow direction of Fig.7a

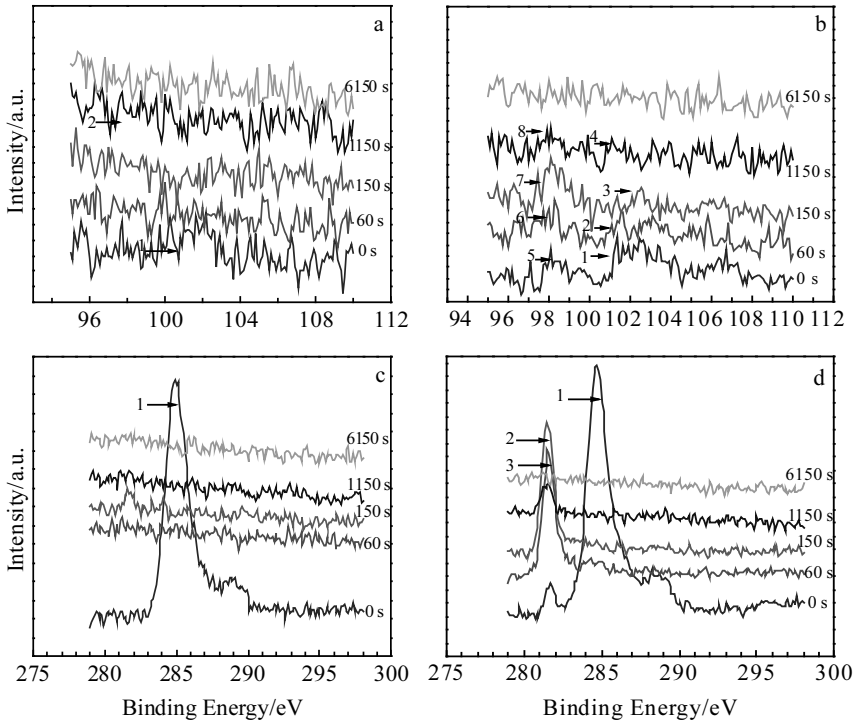

Fig.9 Si and C fine spectra of pickled and un-pickled samples etched for different time: (a) Si-pickled sample, (b) Si-un-pickled sample, (c) C-pickled sample, and (d) C-un-pickled sample

value affect the distribution of second phase particles of Zr-4 alloy and further affect its corrosion resistance, Anada[27] pointed out that if the *A* value is insufficient, there will be a large number of fine second phase particles in the sheet samples. As shown in Fig.10a and 10c, Fe and Cr in these fine particles easily diffuse into the surrounding ZrO_2 oxide layer to form FeO and Cr_2O_3, resulting in local stress increase in the oxide layer. The columnar structure of local ZrO_2 oxide film will be destroyed and begin to transform into fine equiaxed structure. As shown in Fig.10e and 10g, further evolution will

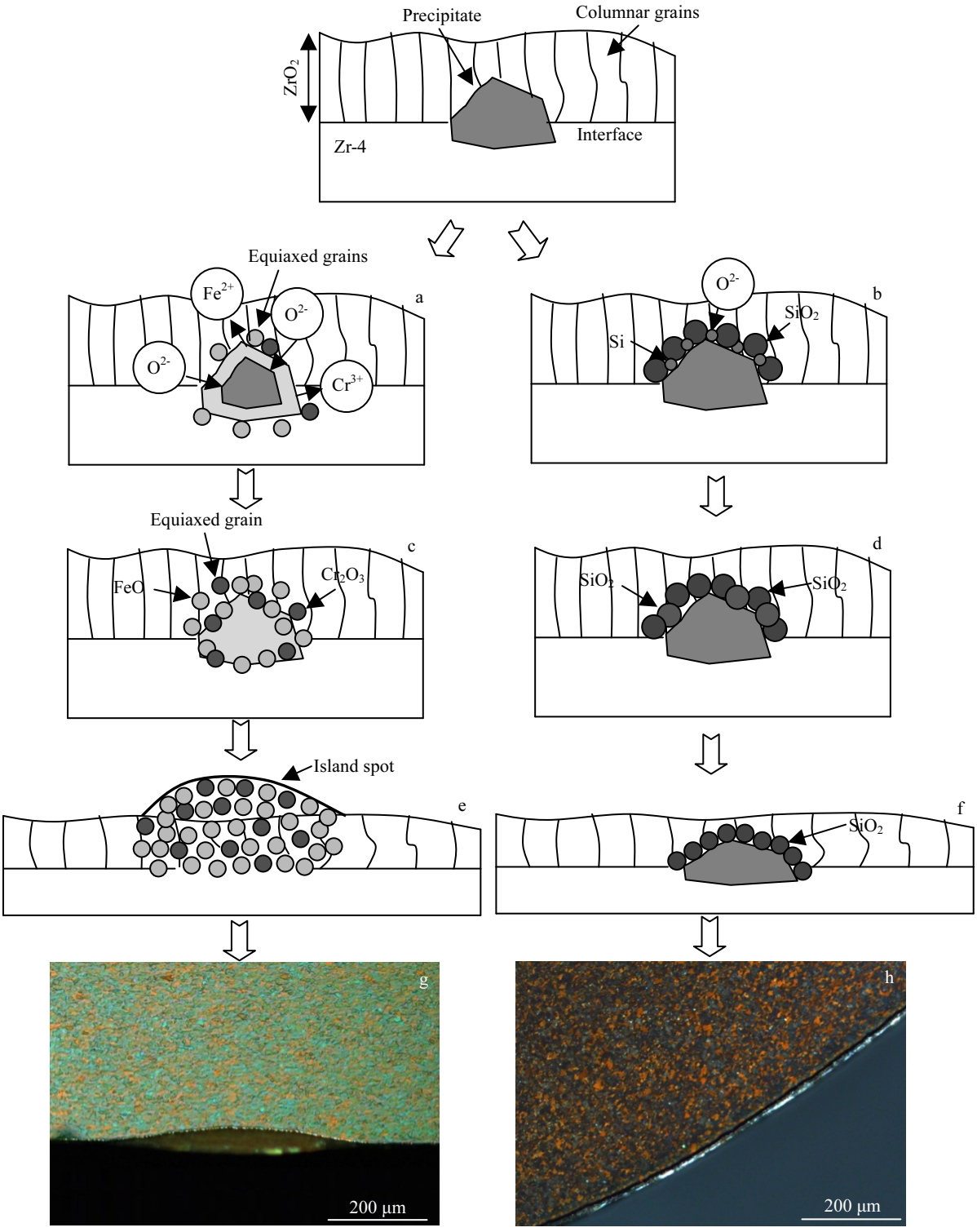

Fig.10 Effect of silicon contents on the second phase particles: (a, c, e, g) low Si content and (b, d, f, h) high Si content

result in macroscopic local 'island' spots. Correspondingly, it shows the higher corrosion mass gain than the samples of fine equiaxed structure.

In this paper, it is considered that the corrosion resistance of Zr-4 alloy is closely related to the distribution of second phase particles. On the one hand, improvement of corrosion resistance can be achieved by increasing the precipitation quantity and size of second phase particles, for example, increasing the cumulative annealing parameter (*A* value), but this may deteriorate nodular corrosion resistance. On the other hand, it can also be realized by providing an 'isolation layer' for precipitating fine second phase particles to delay or weaken their oxidation rate, thus giving consideration to corrosion performance. As shown in Fig.10b and 10d, microanalysis shows that SiO_2 and Si enriched around the second phase particles can isolate the fine particles from the outside O^{2-}, and prevent Fe and Cr from being diffused and oxidized. As shown in Fig.10f and 10h, the columnar crystal structure of the ZrO_2 oxide film is maintained effectively, and thus the thickness of oxide film is uniform and consistent.

3 Conclusions

1) Reducing Sn content and increasing Fe+Cr content are beneficial to uniform corrosion performance of Zr-4 alloy at 400 °C steam. Taking into account the control difficulty of industrial production, the key to obtain Zr-4 alloy products with excellent corrosion resistance is to reduce the C content and increase Si content.

2) Carbon is easily enriched in the form of Zr-C on the matrix surface, and its content mainly affects the corrosion resistance by affecting the precipitation of second phase particles.

3) Silicon tends to agglomerate in the form of SiO_2 around the second phase particles, and plays a role in delay or weaken the oxidation of second phase particles, thus improving the corrosion resistance of Zr-4 alloy.

4) Compared to increasing the cumulative annealing parameter (*A* value), it is more suitable to use the 'low C content and high Si content' component to obtain the Zr-4 alloy products with excellent corrosion resistance.

References

1 Li Shilu, Yao Meiyi, Zhang Xin *et al*. *Acta Metallurgica Sinica* [J], 2011, 47(2): 163 (in Chinese)

2 Yao Meiyi, Li Shilu, Zhang Xin *et al*. *Acta Metallurgica Sinica*[J], 2011, 47(7): 865 (in Chinese)

3 Zhang Xin, Yao Meiyi, Peng Jianchao *et al*. *Rare Metal Materials and Engineering*[J], 2017, 46(12): 3910 (in Chinese)

4 Yang Zhongbo, Cheng Zhuqing, Qiu Jun *et al*. *Rare Metal Materials and Engineering*[J], 2018, 47(3): 794

5 Xue Xiangyi, Bai Xinde, Liu Jianzhang *et al*. *Rare Metal Materials and Engineering*[J], 2005, 34(1): 64

6 Yao M Y, Wu X T, Huang J *et al*. *Oxidation of Metals*[J], 2015, 84(5-6): 647

7 Guo Xiaopan, Zhang Jinlong, Chen Bin *et al*. *The Chinese Journal of Nonferrous Metals*[J], 2018, 28(2): 340 (in Chinese)

8 Hou Keke, Huang Jiao, Yao Meiyi *et al*. *Rare Metal Materials and Engineering*[J], 2019, 48(5): 1440

9 Liang Nan, Zhang Jinlong, Yuan Gaihuan *et al*. *Rare Metal Materials and Engineering*[J], 2017, 46(1): 201 (in Chinese)

10 Yao Meiyi, Zou Linhong, Xie Xingfei *et al*. *Acta Metallurgica Sinica*[J], 2012, 48(9): 1097 (in Chinese)

11 Kirsty Annand, Magnus Nord, Ian Maclaren *et al*. *Corrosion Science*[J], 2017, 128 (14): 213

12 Li Qiang, Ma Shuai, Yang Yanping *et al*. *Rare Metal Materials and Engineering*[J], 2018, 47(9): 2761 (in Chinese)

13 Thorvaldsson T, Andersson T, Wilson A *et al*. *8th International Symposium on Zirconium in the Nuclear Industry*[C]. Philadelphia: ASTM, 1989: 128

14 Charquet D, Alheritiere E. *7th International Symposium on Zirconium in the Nuclear Industry*[C]. Philadelphia: ASTM, 1987: 284

15 Maussner G, Steinberg E, Tenckhoff E. *7th International Symposium on Zirconium in the Nuclear Industry*[C]. Philadelphia: ASTM, 1987: 307

16 Garzarolli G, Steinberg E, Weidinger H G. *8th International Symposium on Zirconium in the Nuclear Industry*[C]. Philadelphia: ASTM, 1989: 202

17 Foster John P, Anada Hiroyuki. *10th International Symposium on Zirconium in the Nuclear Industry*[C]. Philadelphia: ASTM, 1994: 307

18 Sabol G P. In: Rudling P, Kammenzind B eds. *14th International Symposium on Zirconium in the Nuclear Industry*[C]. Philadelphia: ASTM, 2004: 3

19 Cao Xiaoxiao, Yao Meiyi, Peng Jianchao *et al*. *Acta Metallurgica Sinica*[J], 2011, 47(7): 882 (in Chinese)

20 Eucken C M, Finden P T, Trapp-Pritsching S *et al*. *8th International Symposium on Zirconium in the Nuclear Industry*[C]. Philadelphia: ASTM, 1989: 113

21 Luan Baifeng, Xue Jiaojiao, Chai Linjiang *et al*. *Rare Metal Materials and Engineering*[J], 2013, 42(12): 2636

22 Rudling P, Pettersson H, Andersson T *et al*. *8th International Symposium on Zirconium in the Nuclear Industry*[C]. Philadelphia: ASTM, 1989: 213

23 Andersson T, Vesterlund G. *5th International Symposium on Zirconium in the Nuclear Industry*[C]. Philadelphia: ASTM, 1982: 75

24 Wadman B, Andren H O. *9th International Symposium on Zirconium in the Nuclear Industry*[C]. Philadelphia: ASTM, 1991: 461

25 Godlewski J. *10th International Symposium on Zirconium in the Nuclear Industry*[C]. Philadelphia: ASTM, 1994: 663

26 Chai Linjiang, Luan Baifeng, Chen Jianwei *et al*. *Rare Metal Materials and Engineering*[J], 2012, 41(6): 1119 (in Chinese)

27 Anada H, Herb B J, Nomoto K *et al*. *11th International Symposium on Zirconium in the Nuclear Industry*[C], Philadelphia: ASTM, 1996: 74

杂质元素（C, Si）对 Zr-4 合金板材微观结构及耐腐蚀性能的影响

储林华[1]，袁改焕[1]，姚美意[2]，高　博[1]，徐诗彤[2]，周邦新[2]

(1. 国核宝钛锆业股份公司 国家能源核级锆材研发中心 陕西省核级锆材重点实验室，陕西 宝鸡 721013)

(2. 上海大学，上海 200072)

摘　要：在 ASTM 标准范围内，利用板材试样研究了杂质元素对 Zr-4 合金微观结构和耐腐蚀性能的影响。结果表明，降低 C 含量、提高 Si 含量，有利于改善 Zr-4 合金在 400 ℃蒸汽下的耐均匀腐蚀性能。微观分析显示，元素 C 易于以 Zr-C 形式在基体相表面富集，其主要通过左右第二相粒子的析出进而影响耐腐蚀性能。C 含量越低，淬火过程中坯料越倾向于形成平行板条（PP）结构；C 含量越高，越易于形成网篮（BW）结构；而第二相粒子更易于沿平行板条结构的边界析出。当淬火温度低于 1200 ℃时，Si 含量对于是否形成平行板条结构没有明显影响。同时，三维原子探针（3DAP）分析显示，Si 倾向于以 SiO_2 形式在第二相粒子周围偏聚，推迟或延缓了第二相粒子的氧化过程，进而提升了 Zr-4 合金的耐腐蚀性能。

关键词：锆合金；杂质；微观组织；均匀腐蚀；β 相固溶处理；第二相粒子；偏聚

作者简介：储林华，男，1984 年生，博士，高级工程师，国核宝钛锆业股份公司，陕西 宝鸡 721013，电话：0917-8661613，E-mail: chulinhuascu@163.com